Three-Dimensional Polymeric Microtiles for Optically-Tracked Fluidic Self-Assembly

Massimo Mastrangeli[a,b,1,*], Alcherio Martinoli[b], Juergen Brugger[a]

[a]*Microsystems Laboratory (LMIS1), Institute of Microengineering, School of Engineering, École Polytechnique Fédérale de Lausanne (EPFL), Station 17, 1015 Lausanne, Switzerland*
[b]*Distributed Intelligent Systems and Algorithms Laboratory (DISAL), School of Architecture, Civil and Environmental Engineering, École Polytechnique Fédérale de Lausanne (EPFL), Station 2, 1015 Lausanne, Switzerland*

Abstract

Self-assembly (SA) is a bio-inspired key coordination mechanism for swarms of intelligent agents as well as a pervasive bottom-up methodology for the fabrication of heterogeneous micro- and nanosystems. Analytical studies of SA at small scales are therefore highly relevant for many technological applications. In this paper we present an innovative design and fabrication process for three-dimensional polymeric microtiles conceived as passive vehicles to investigate the dynamics of fluidic SA at sub-millimeter scale. The microtiles are fabricated out of the superposition of two structural SU-8 layers featuring chiral copies of the same centro-symmetric pattern. They can coordinate laterally in water independently of their vertical orientation to form close-packed square lattice clusters. The microtiles embed a central marker enabling the real-time optical tracking and automated closed-loop control of their fluidic SA. The fabrication process makes use of a thick sacrificial copper layer and allows the wafer-level batch production of tens of thousands of microtiles, in line with the massively parallel nature of SA.

[*]Corresponding author

Email addresses: `mastrangelim@gmail.com` (Massimo Mastrangeli), `alcherio.martinoli@epfl.ch` (Alcherio Martinoli), `juergen.brugger@epfl.ch` (Juergen Brugger)

[1]Present address: Bio-, Electro- And Mechanical Systems (BEAMS) Department, École Polytechnique, Université Libre de Bruxelles, CP 165/56, Avenue Franklin D. Roosevelt 50, B-1050 Bruxelles. Tel.: +32 (0) 2 650 47 66; Fax.: +32 (0) 2 650 24 82

1. Introduction

Self-assembly (SA) is the autonomous formation of ordered structures out of the spatial organization of their components [1]. Both in SA and in standard manufacturing, the information required to assemble target structures is known a priori [2]. Yet in SA this information is not centralized into an external supervisor or planner, but rather distributedly encoded within the properties of the interactions taking place 1) among the components and 2) between the components and the environment [3]. For passive components, the interactions can be controlled by tailoring their shape, material composition and surface properties with respect to the phase (liquid or gaseous) hosting the assembly. Active components can additionally move autonomously, share information through communication networks and make decisions about interactions. The components can alternatively scavenge mobility from the environment. The latter can also include templates or other physical means to constrain the stochastic dynamics of the system. Interactions and environment catalyze or direct the evolution of the system toward the configuration of minimal energy corresponding to the desired assembly. SA is a form of chemistry, whereby assemblies among components correspond to reactions among reactants and punctuate the progress of the stochastic process [4]. SA can take place at all spatial scales given proper boundary conditions [5]. At each scale, several differing implementations of SA are possible [6, 7] and are normally scale-specific. Scale specificity is due, among many factors, to the scaling laws of body versus surface forces [8], to the associated scale dependence of sensing, actuation and manufacturing techniques, and to the consequent trade-off between component sophistication and size [2].

Thanks to these notable features, SA is central to both advanced manufacturing and swarm robotics. SA represents a pervasive, bottom-up and massively parallel methodology for the fabrication of heterogeneous micro- and nanobiosystems [6, 2, 9]. It is also a key coordination task for distributed robotic systems, especially those consisting of a large number of nodes [7, 10]. SA may ultimately bridge these two domains, particularly for millimetric- to micrometric-sized components [11]. In this scale range, surface forces dominate, and a broad variety of innovative functional systems has been assembled

by a combination of fluidic drag and surface tension forces, *i.e.* by fluidic SA [12, 13]. Analytic studies on the dynamics and control of SA at this scale are therefore pivotal for further technological advances. Yet to date they remain scarce compared to experimental proofs of concepts [11].

In this paper we present an innovative design and fabrication process for three-dimensional polymeric microtiles. The microparticles are conceived as passive vehicles to investigate the dynamics of fluidic SA at sub-millimeter scale—as an extension of our previous studies at centimeter scale [14]. The microtiles are fabricated out of the superposition of two structural layers of SU-8 [15] representing chiral copies of the same four-fold symmetric pattern. They can by design coordinate laterally in water through hydrophobic interactions and shape matching independently of their vertical orientation to form close-packed, square lattice clusters. The microtiles feature a central marker aiding the real-time optical tracking and automated closed-loop control of their fluidic SA [16] performed by a dedicated platform [17]. The fabrication process makes use of copper as thick sacrificial layer and allows the wafer-level production of tens of thousands of microtiles in a single batch—in line with the massively parallel and scalable nature of SA.

2. Materials and Methods

2.1. Design of the Microtiles

SA entails the spatial coordination of components into extended structures. Three- and two-dimensional components are normally designed with polyhedral [18] and polygonal [13] symmetrical shapes, respectively. This makes the topology of the stochastically assembled structures more predictable and easier to control—particularly for populations with components of a unique type. The SA of polygonal components over a two-dimensional (2D) space resemble a tessellation process [19] to form clusters with predefined lattice structure. Tile-like 2D components with regular polygonal shapes such as triangles [20, 21, 22], squares [23] and hexagons [24] are especially common in literature. Components with more elaborate geometries have nonetheless been used [19, 25, 26, 27, 28], as well as ensembles of multiple types of components with mutually orthogonal [29] or uniquely encoded shapes [30] designed to avoid mutual interference during concurrent assembly onto patterned substrates.

In an earlier study of fluidic SA at centimeter scale, we designed passive blocks with four-fold in-plane rotational symmetry [14]. The blocks floated at
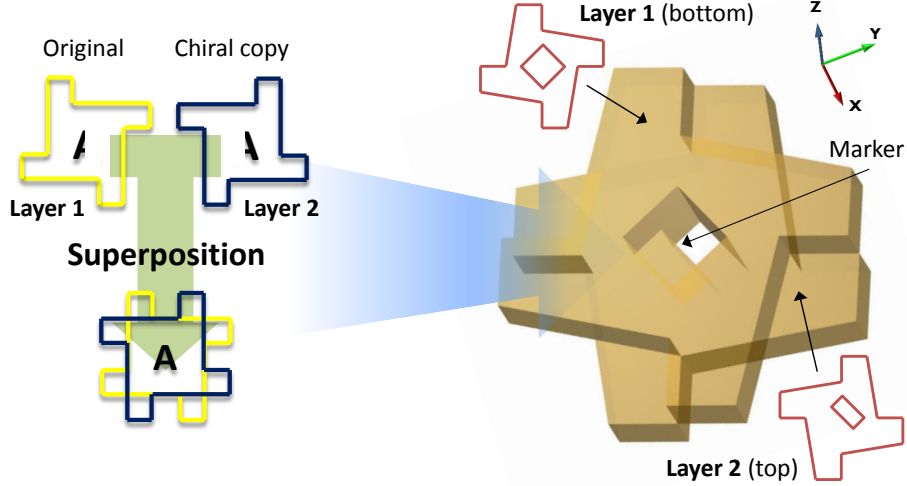
Figure 1: Conception and design of the three-dimensional microtiles by superposition of chiral geometrical shapes.

the water/air interface and could preserve their vertical orientation throughout entire assembly realizations. The geometric profile, also adopted by Tolley for sub-millimetric components [23], was functional to the self-alignment and latching of the blocks upon close approach. The blocks could coordinate into a finite variety of square lattice structures with predictable topology. We aimed at adopting an analog geometry for our microscopic vehicles. However, in the corresponding microfluidic platform [17] the microtiles are completely immersed in a single liquid phase and cannot be constrained to preserve their initial vertical orientation indefinitely. As a consequence, even assuming an initial population of identically oriented microtiles, two subpopulations with opposite orientations, *i.e.* microtiles with chiral copies of the same geometrical shape, are expected to rapidly appear. The two populations would then not be able to interact and spatially coordinate properly, as this requires the matching of the sides of the microtiles. We remark that this issue is not specific to our design, rather it affects all 2D shapes with central inversion symmetry. Getting rid of the latter would solve the problem at the cost of renouncing to the advantages mentioned above, namely lateral alignment and predictable topology.

We therefore adopted a design solution based on the vertical superposition of the chiral copies of the original shape (Fig. 1). This geometry allows tight
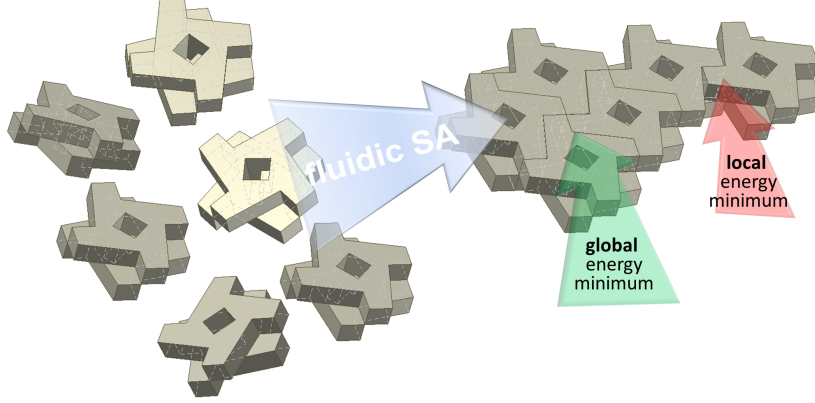
4

Figure 2: Fluidic SA of the microtiles. Assembly configurations corresponding to global and local energy minima are evidenced.

matching among contacting microtiles independently of their vertical orientation (Fig. 2). The resulting three-dimensional microtiles are non-uniform along the vertical axis, in contrast to all examples cited earlier. Furthermore, the bi-layered geometry more than doubles the total interaction area between close-packed matching microtiles. The contact can in fact take place both horizontally, along the vertical sidewalls, and vertically, along the suspended protrusions of each layer. The increment in contact area is particularly advantageous since the microtiles are immersed in bulk water and the assembly is thereby driven by surface forces such as hydrophobic interactions [31] and fluidic drag [32]. Finally, the design includes a central bichromatic optical marker in the form of a double step engraved in the structural layers of the microtiles. The geometrical marker exploits the difference in optical reflectivity between structural layers of different thickness, specifically between null (*i.e.* through-hole) and single-layer thickness. The marker is thus embedded in the microtiles without the use of additional patterning or coloring. The marker is introduced to ease the optical tracking of the microtiles performed by a dedicated software framework based on the SwisTrack suite [33].

2.2. Fabrication Process

We aimed for a batch, wafer-scale fabrication process for polymeric microtiles, consistent with the massively parallel nature of SA. We thus did not consider direct-write, layer-by-layer fabrication techniques such as micro 3D printing [34] as an option, though they may be able to fabricate individual
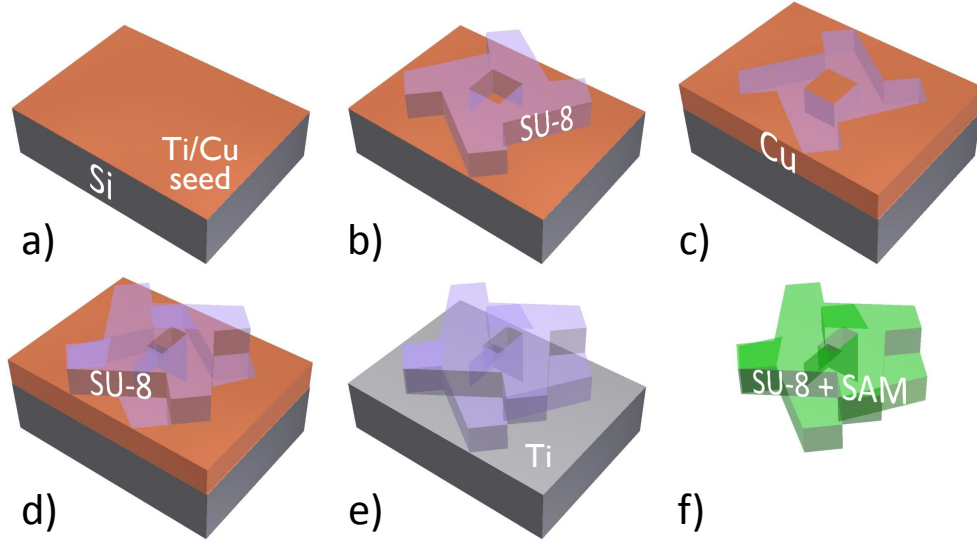
5

Figure 3: Process steps for the wafer-level fabrication of the microtiles (see text for details).

microtiles with adequate resolution.

2D microtiles (Sect. 2.1) can be produced through a single lithographical patterning step. Conversely, even using a negative tone epoxy resist such as SU-8 [15] as structural material the articulated 3D geometry of our microtiles requires a more elaborate fabrication process. The reason is found in the only partial superposition of the two structural layers—said equivalently, in the presence of portions of the top layer that are suspended and do not overlap with counterparts in the bottom layer. Bonding of the two layers, each priorly patterned on a separate substrate, can represent a fabrication option. This option is cumbersome though, as it requires precise wafer-to-wafer alignment and possibly the use of at least one glass wafer out of the two for bonding purposes. Alternatively, an optically opaque layer may be introduced between the sequentially spun structural layers to ideally avoid cross exposures between them. Yet notably, an intermediate layer is not straightforwardly compatible with the geometrical shape matching embedded in our microtile design. Besides, introducing such stopping layer without adverse consequences is practically not trivial, as it would require an additional patterning step, complicate alignments and possibly hinder the correct definition or development of the bottom structural layer. Double-sided masked etch of silicon-on-insulator (SOI) wafers exploiting the buried oxide as built-in etch
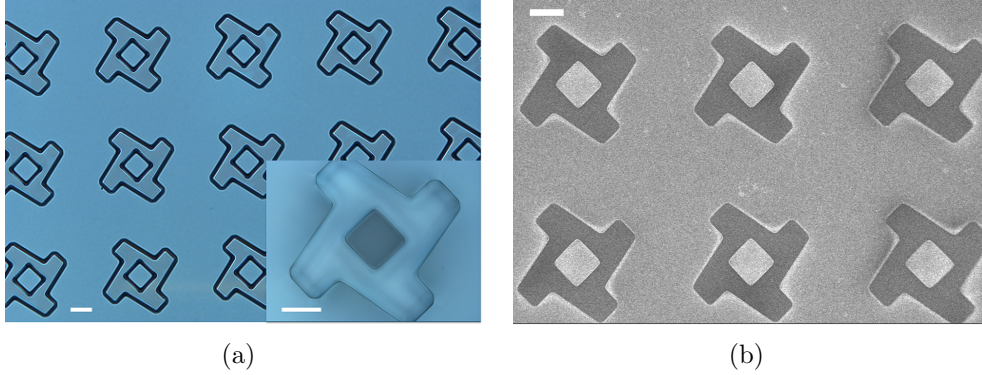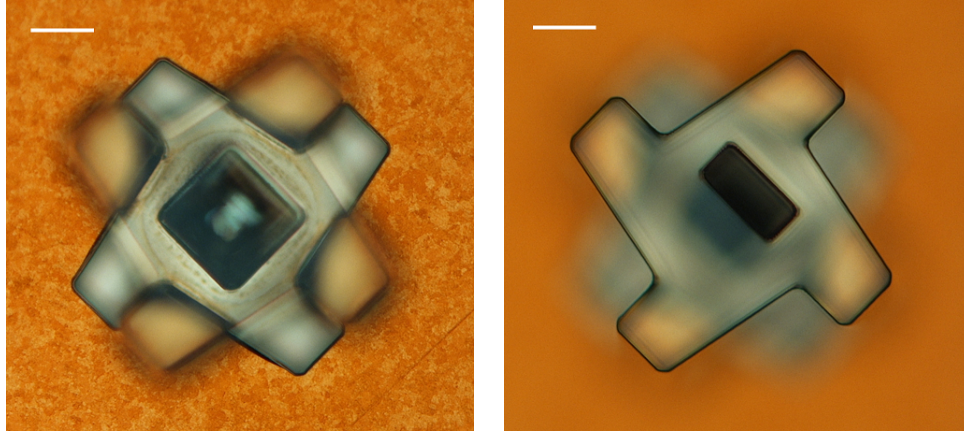
Figure 4: Processing of the bottom layer of the microtiles. (a) Optical picture of the patterned SU-8 layer. (b) SEM micrograph of the SU-8 layer embedded into electroplated Cu and before CMP. Scale bars are 50 μm.

stop layer could represent an elegant fabrication path for silicon-based microtiles. Yet such approach would also 1) require precise wafer grinding and thinning, and possibly pose more restrictions on the thickness of the structural layers, 2) need to deal with the intermediate layer similarly as above, 3) be challenging for microtiles handling, and 4) be more expensive.

As shown in Fig. 3 and detailed below, we alternatively opted for a simpler though non-standard SU-8-centered fabrication process whereby electroplated copper is used as thick sacrificial layer. An arbitrarily-thick sacrificial layer can be grown by copper electroplating that can: 1) conformally embed a pre-patterned (bottom) structural layer, 2) allow surface leveling prior to subsequent deposition and patterning of the top structural layer, and 3) be easily etched away. Microtiles with 210 μm diameter as well as three downscaled versions with identical geometry (5%, 10% and 15% smaller, respectively) are fabricated on each batch.

To start the microfabrication process, a 100 mm Si wafer is dehydrated at 100 ^{o}C in an oven prior to the evaporation of a Ti/Cu seed layer (50 and 100 nm-thick, respectively; Fig. 3a). After a subsequent dehydration step the Cu surface is spin-coated with a 47 μm-thick layer of SU-8 (GM 1070, Gersteltec) which is soft-baked at a maximum temperature of 100 ^{o}C and left to relax overnight to improve surface leveling across the substrate. The SU-8 layer is then processed by proximity UV lithography through a chromium mask for geometrical patterning. The exposure parameters (33 s, 8 mW/cm^2) were optimized to account for the reflectivity of the Cu surface.

(a) Top surface of bottom SU-8/Cu layer.　　(b) Top surface of top SU-8 layer.

Figure 5: Geometry of the two SU-8 structural layers of a microtile embedded in the Cu sacrificial layer. Distance between focal planes is about 50 μm. Scale bars are 50 μm.

The geometry of this SU-8 layer features a central square hole (70 μm in side) as part of the optical marker pattern. After post-exposure bake at 130 ^{o}C, the SU-8 layer is developed in PGMEA, rinsed in isopropyl alcohol and slowly dryed by evaporation under laminar air flow (Fig. 3b and 4a). Native oxides are then removed from the surface of the Cu seed layer through a brief etch in sulfuric acid, and Cu electroplating is performed in a recirculating Cu bath whose composition (Cu sulfate, sulfuric acid, chlorure and additives) is adapted from Rohm & Haas Intervia 8520. Cu growth needs to be slow enough to avoid the inclusion of voids within the Cu layer in proximity of the sidewalls of the SU-8 layer. A Cu growth rate of about 1.1 μm/s was obtained for a current density of 45 mA/cm^2 at a bath temperature of 27 ^{o}C. Still, precise control over the final thickness of the electroplated Cu layer could not be achieved. Thickness variations as large as 10 μm were measured by mechanical profilometry across the wafers, the peripheral wafer regions being thicker than the inner ones possibly due to edge effects. Local Cu overgrowth was also measured in proximity of the microtiles. According to this evidence, Cu electroplating alone can not be used to level the composite Cu/SU-8 surface. To achieve the purpose, we hence resorted to Cu over-plating (about 55 μm-thick Cu layer after 50 minutes) followed by a delicate chemical mechanical polishing (CMP) step (Fig. 3c and 4b). CMP on the mixed Cu/SU-8 matrix is performed for 1 hour using a Cu-dedicated setup
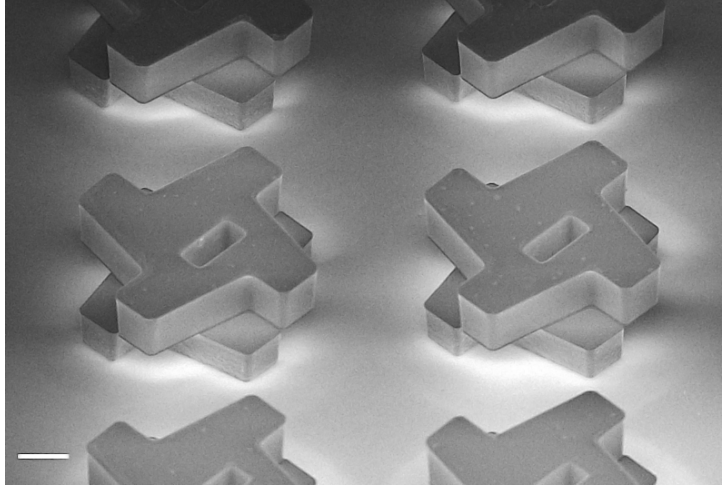
Figure 6: SEM micrograph of the SU-8 microtiles after etch of the sacrificial Cu layer. Scale bar is 50 μm.

with parameters adapted from Cu processing (slurry of 12 nm silica particles (3% wt.) and pH 2.2; applied pressure of 5 psi; plate and head speed of 90 rpm). Post-CMP mechanical profilometry measured a final thickness variation smaller than 0.5 μm, the best results locally concentrated in the center of the wafer. The post-CMP thickness of the SU-8/Cu layer was larger than 45 μm. The second SU-8 layer is subsequently deposited and lithographically patterned on the leveled surface (Fig. 3d). The same procedure as for the first layer is used. The Cu/SU-8 surface (Fig. 5a) is priorly activated by exposure to mild oxygen plasma (100 W, 2 minutes) to enhance SU-8 adhesion and bonding. The pattern of the second SU-8 layer features a central rectangular hole superposed on a side of the central square hole of the first layer, and with half its dimension (Fig. 5b). The vertical combination of the two holes determines the optical marker. The Cu layer is then removed by immersing the substrate into a Cu etch bath ($(NH_4)_2S_2O_8+H_2SO_4$ (96%), 60 g/L and 10 mL/L, respectively; etch rate: 200 nm/s) for about 5 hours (Fig. 3e). The exposed SU-8 surfaces of the microtiles (Fig. 6) are then treated with oxygen plasma as before and functionalized with trichloro (1H, 1H, 2H, 2H-perfluorooctyl)silane self-assembled monolayer (SAM) deposited from vapor phase to increase their hydrophobic character. The microtiles are finally released from the substrate by ultrasonication (35 kHz, 5 s) in de-ionized water (Fig. 3f).
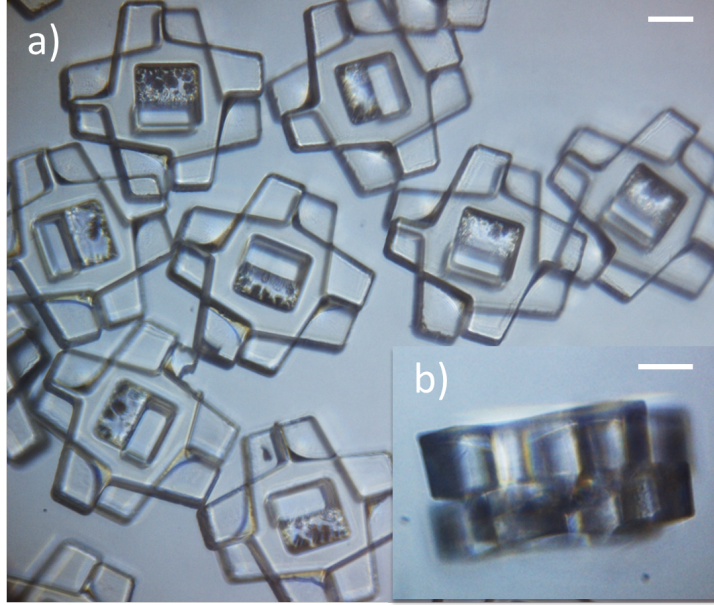
Figure 7: Release of the microtiles. a) Microtiles released in water by ultrasonication. b) Side view of a microtile. Scale bars are 50 μm.

3. Results and discussion

Figure 7a shows the microtiles in water after release. The fabricated shape well matches the conceived design. Notably, apart from the exception mentioned below, all surfaces are very smooth and straight as required. The central bichromatic marker is clearly distinguishable within the body of the microtiles, as well.

Roughness and residual traces of Cu are detectable only in the half part of the marker composed by a single SU-8 layer. As described in Sect. 2.2, that SU-8 part was spun and patterned above the Cu layer grown inside the central square hole of the bottom layer. This geometry locally limited the diffusion of the etchant and therefore slowed down the rate of Cu etch within the central marker, as sketched in Fig. 8a. As a result, by the time the sacrificial Cu layer filling the space among the microtiles was completely removed—thus exposing the surface of the underlying Ti layer—the microtiles did not detach from the substrate. Instead, they held onto residual microposts of unetched Cu hidden below the central marker (Fig. 8b). Array of Cu microposts were indeed clearly seen on the substrate upon release of the microtiles (Fig. 8c).
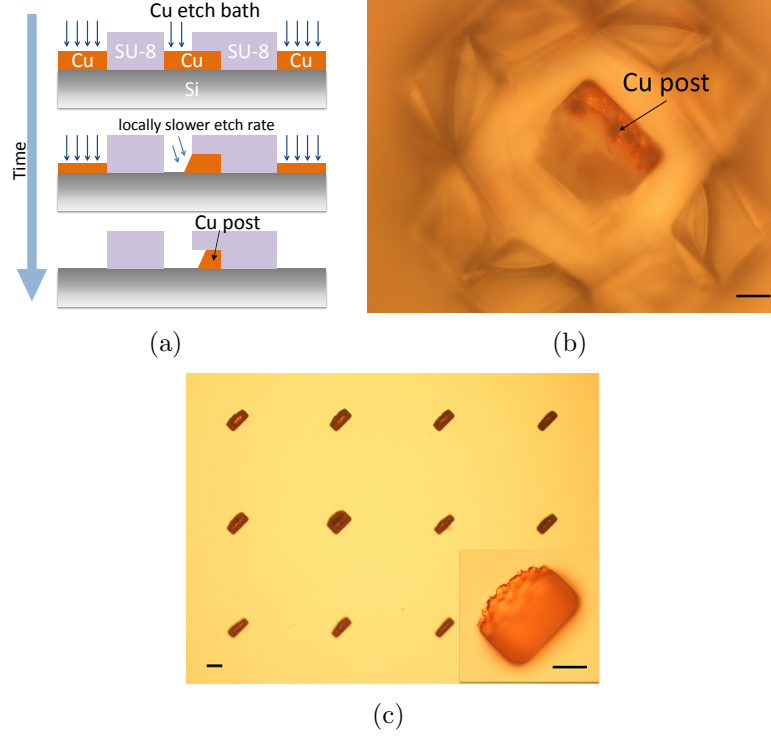
Figure 8: Anchoring of the microtiles on the substrate after Cu etch. (a) Sketch of the formation of a residual Cu micropost within a microtile (cross-sectioned, not in scale) during etch of the sacrificial Cu layer. (b) Microtile anchored to a Cu micropost after Cu etch. (c) Cu posts residual onto Ti surface after release of the microtiles. Scale bars are 25 μm.

Such post-Cu etch anchoring of the microtiles onto the substrate permitted the SAM deposition from vapor phase. The former is easier compared to alternative SAM deposition from liquid phase, although it leaves the bottom side of the microtiles unfunctionalized.

The microfabrication yield approaches 100% across the full wafer. Microtiles featuring only a rectangular central marker, *i.e.* composed of the single top layer, are sporadically detected in water upon release by ultrasonication. This is evidence of locally-poor adhesion and bonding of the top SU-8 layer onto the bottom one. Local defects or uncleanliness of the surface of the latter could prompt this very rare failure mode. Additionally, side views of a few of the released microtiles (see for instance Fig. 7b) show a slight difference in thickness between the superposed SU-8 layers. The difference
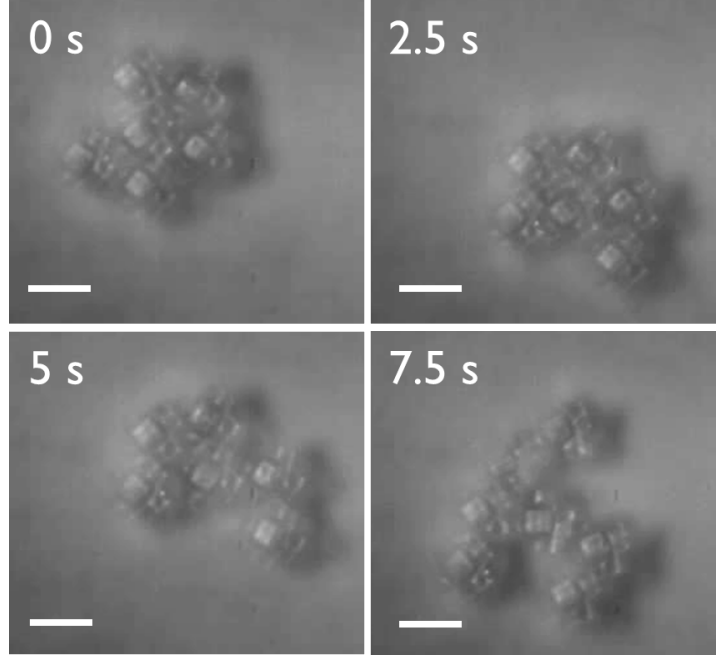
11

Figure 9: Frames from a high-speed recording of the SU-8 microtiles in bulk water [17] self-assembling into crystalline clusters of varying topology. Scale bar is 200 μm.

is mainly attributed to the thinning of the bottom SU-8 layer induced by the CMP step and could be expected from the profilometric measurements reported in Sect. 2.2.

Finally, fluidic SA experiments performed in the dedicated acousto-fluidic platform [17] (Fig. 9) evidence that neither the uncomplete SU-8 derivatization through the vapor-deposited SAM nor the slight asymmetry in layer thickness of some of the microtiles appear to significantly affect the SA dynamics of the microtiles. The latter depends significantly on the assembly technique and control strategy adopted, and is described in depth in [16].

4. Conclusions

We presented an innovative design and corresponding non-standard microfabrication process for three-dimensional polymeric microtiles suited for the investigation of microfluidic SA. The design solves the assembly issue related to the unpredictable vertical orientation of the microtiles within a bulk liquid phase. The tailored fabrication process makes use of a thick Cu

sacrificial layer to allow for the independent patterning of two superposed SU-8 structural layers, and can be upscaled to large substrates for the batch production of very large quantities of microtiles. This work is crucial toward in-depth experimental studies and analytical modeling of SA at microscale [16], which can benefit the expanding classes of advanced robotic and micro/nanomanufacturing technologies adopting SA as core paradigm.

Acknowledgments

[1] B. Grzybowski, C. E. Wilmer, J. Kim, K. P. Browne, K. J. M. Bishop, Self-assembly: from crystals to cells, Soft Matter 5 (2009) 1110–1128.

[2] M. Boncheva, G. M. Whitesides, Making things by self-assembly, MRS Bullettin 30 (2005) 736–742.

[3] T. Hogg, Robust self-assembly using highly designable structures, Nanotechnology 10 (1999) 300–7.

[4] G. Mermoud, Stochastic Reactive Distributed Robotic Systems: Design, Modeling and Optimization, Vol. 93 of Springer Tracts in Advanced Robotics, Springer, 2014.

[5] G. B. Whitesides, B. Grzybowski, Self-assembly at all scales, Science 295 (2002) 2418–2421.

[6] M. Mastrangeli, S. Abbasi, C. Varel, C. van Hoof, J.-P. Celis, K. F. Bohringer, Self-assembly from milli- to nanoscale: methods and applications, J. Micromech. Microeng. 19 (2009) 083001.

[7] R. Gross, M. Dorigo, Self-assembly at the macroscopic scale, Proc. IEEE 96 (2008) 1490–1508.

[8] W. S. N. Trimmer, Microrobots and microelectromechanical systems, Sensor. Actuator. 19 (1989) 267–287.

[9] T. G. Leong, A. M. Zarafshar, D. H. Gracias, Three-dimensional fabrication at small size scales, Small 6 (2010) 792–806.

[10] G. Mermoud, A. Prorok, L. Matthey, C. M. Cianci, N. Correll, A. Martinoli, Handbook of collective robotics: Fundamentals and challenges, Pan Stanford Publishing, 2013, Ch. Self-Organized Robotic Systems: Large-Scale Experiments in Aggregation and Self-Assembly using Miniature Robots, pp. 229–259.

[11] M. Mastrangeli, G. Mermoud, A. Martinoli, Modeling self-assembly across scales: The unifying perspective of Smart Minimal Particles, Micromachines 2 (2011) 82–115.

[12] N. B. Crane, O. Onen, J. Carballo, Q. Ni, R. Guldiken, Fluidic assembly at the microscale: progress and prospects, Microfluid. Nanofluid. 14 (2013) 383–419.

[13] M. Mastrangeli, Surface tension in microsystems, Springer, 2013, Ch. Surface tension-driven self-assembly, pp. 227–253.

[14] G. Mermoud, M. Mastrangeli, U. Upadhyay, A. Martinoli, Real-time automated modeling and control of self-assembling systems, in: 2012 IEEE Int. Conf. on Robotics and Automation, 2012, pp. 4266–4273.

[15] H. Lorenz, M. Despont, N. Fahrni, J. Brugger, P. Vettiger, P. Renaud, High-aspect-ratio, ultrathick, negative-tone near-UV photoresist and its applications for MEMS, Sens. Actuators A: Physical 64 (1998) 33–39.

[16] M. Mastrangeli, F. Schill, J. Goldowsky, H. F. Knapp, J. Brugger, A. Martinoli, Automated real-time control of fluidic self-assembly of microparticles, in: 2014 IEEE Int. Conf. on Robotics and Automation, 2014.

[17] J. Goldowsky, M. Mastrangeli, L. Jacot-Descombes, M. R. Gullo, G. Mermoud, J. Brugger, A. Martinoli, B. J. Nelson, H. F. Knapp, Acousto-fluidic system assisting in-liquid self-assembly of microcomponents, J. Micromech. Microeng. 23 (2013) 125026.

[18] S. Pandey, M. Ewing, A. Kunas, N. Nguyen, D. H. Gracias, G. Menon, Algorithmic design of self-folding polyhedra, Proc. Natl. Acad. Sci. 108 (2011) 19885–19890.

[19] P. Rothemund, Using lateral capillary forces to compute by self-assembly, Proc. Natl. Acad. Sci. 97 (2000) 984–989.

[20] K. Hosokawa, I. Shimoyama, H. Miura, Two-dimensional micro-self-assembly using the surface tension of water, Sensor. Actuat. A-Phys. 57 (1996) 117–125.

[21] E. Klavins, Programmable self-assembly, IEEE Contr. Syst. Mag. 24 (2007) 43–56.

[22] S. Miyashita, M. Göldi, R. Pfeifer, How reverse reactions influence the yield of self-assembly robots, Int. J. Rob. Res. 30 (2011) 627–641.

[23] M. T. Tolley, K. M., D. Erickson, H. Lipson, Dynamically programmable fluidic assembly, Appl. Phys. Lett. 93 (2008) 254105.

[24] N. Bowden, I. S. Choi, B. A. Grzybowski, G. M. Whitesides, Mesoscale self-assembly of hexagonal plates using lateral capillary forces: synthesis using the 'capillary bond', J. Am. Chem. Soc. 121 (1999) 5373–5391.

[25] U. Srinivasan, D. Liepmann, R. T. Howe, Microstructure to substrate self-assembly using capillary forces, IEEE J. Microelectromech. Sys. 10 (2001) 17–24.

[26] K. Sato, K. Ito, S. Hata, A. Shimokohbe, Self-alignment of microparts using liquid surface tension: behaviour of micropart and alignment characteristics, Precis. Eng. 27 (2003) 42–50.

[27] X. Xiong, S.-H. Liang, K. F. Bohringer, Geometric binding site design for surface-tension driven self-assembly, in: IEEE Int. Conf. on Robotics and Automation, 2004, pp. 1141–1148.

[28] M. Poty, G. Lumay, N. Vandewalle, Customizing mesoscale self-assembly with three-dimensional printing, New. J. Phys. 16 (2014) 023013.

[29] S. A. Stauth, B. A. Parviz, Self-assembled single-crystal silicon circuits on plastic, Proc. Natl. Acad. Sci. 103 (2006) 13922–13927.

[30] J. G. F. Tsai, Z. Chen, B. Merriman, J. Chen, S. Nelson, C.-J. Kim, A new bio-molecules decryption protocol using shape-encoded particles (SEP), in: 19th IEEE Int. Conf. on Micro Electro Mechanical Systems, 2006, pp. 138–141.

[31] E. E. Meyer, K. J. Rosenberg, J. Israelachvili, Recent progress in understanding hydrophobic interactions, Proc. Natl. Acad. Sci. 103 (2006) 15739–15746.

[32] W. Zheng, H. O. Jacobs, Fabrication of multicomponent microsystems by directed three-dimensional self-assembly, Adv. Funct. Mater. 15 (2005) 732–738.

[33] T. Lochmatter, P. Roduit, C. Cianci, N. Correll, J. Jacot, A. Martinoli, SwisTrack - a flexible open source tracking software for multi-agent systems, in: IEEE/RSJ Int. Conf. on Intelligent Robots and Systems, 2008, pp. 4004–4010.

[34] H. Lee, N. X. Fang, Micro 3d printing using a digital projector and its application in the study of soft materials mechanics, J. Vis. Exp. 69 (2012) 4457.